Surface-charging and particles aggregation behavior of ascharite

Zhihang Li [1], Yuexin Han [2], Kesheng Zuo [1]

[1] School of Earth Science and Resources, Chang'an University, Xi'an 710054, China

[2] College of Resources and Civil Engineering, Northeastern University, Shenyang110819, China

Corresponding author: neulizhihang@sina.com (Li Zhihang)

Abstract: Surface charging and particles aggregation ascharite are investigated through Zeta potential measurement, XPS analysis, SEM analysis and dissolution experiments. The results show that more Mg^{2+} are removed from ascharite surface after dissolution, which confirms that incongruent dissolution of ions in the case of certain ionic substances like rmagnesium ions, hydroxyl groups and borate ions can lead to a net charge on surface. Isomorphous substitution of Fe^{3+} for Mg^{2+} is also regarded as one factor that causes surface charging behavior, which is in consistent with the experimental data. The dissolution process is analyzed to show more details about the dissolution reactions. The disparity in the bonding energy of B–O and Mg–OH surface groups and the difference in free energy of hydration of surface groups are considered to be the basic reason that lead to incongruent dissolution. Eventually, the effect of surface potential on particles aggregation is analyzed by DLVO theory, indicating that dissolution of ascharite has a detrimental effect on particles dispersion.

Keywords: ascharite, surface charge, incongruent dissolution, particles aggregation

1. Introduction

Boron and its compounds are widely used in chemical and metallurgical industries due to the special physical and chemical properties. China is abundant in boron resources with boron reverses ranking next to Turkey, the USA and Russia (Fu et al., 2015). The borate minerals can be divided into three groups, namely sodium and calcium borate, magnesium borate and borosilicate (Liang et al., 2017). Ascharite is a magnesium-rich borate mineral mainly used as raw material for boron industry in China (Li et al., 2007; Gao et al., 2014). Usually, ascharite is associated with serpentine, and froth flotation is used as an efficient way to separate ascharite from serpentine (Li et al., 2016; Zhu et al., 2015).

Grinding is absolutely a necessary procedure in mineral processing. Several researches show ascharite is prone to forming slime during grinding because of its low hardness. Then the fine ascharite particles will attach to other minerals and interfere with each other (Wei et al., 2013; Gao et al., 2017). Therefore, the ascharite flotation recovery is depressed by mineral particles interaction. This phenomenon is also found in many previous researches. For example, adhesion of serpentine to surfaces of pyrite, chlorite and talc can seriously decrease the flotation recovery of useful minerals (Feng et al., 2012; Zhou et al., 2015; Gallios et al., 2007). Particles interaction is attributed to the deterioration of flotation recovery (Gupta et al., 2011; Liu et al., 2019; Zhao et al., 2015).

All minerals in polar media can develop a charged surface and the source of this charge is most commonly started as being a result of one of four possible mechanisms: 1) the ionization or dissociation of inorganic group take place on solid surface leading to the development of surface charge; 2) the adsorption of ions causes solid surface become charged; 3）incongruent dissolution of ions in the case of certain ionic substances resulting in a net charge on surface; 4) isomorphous substitutions and defects lead to an exchange of one ion for another one with the similar ionic radius (Shaw et al., 1969; Furrer et al., 1988; Vermilyea et al., 1966; Oelkers et al., 1994). References showed that aggregation of minerals particles was closely related to the mineral surface potential, which played an important role in

controlling particle-particle interactions during flotation process (Kusuma et al., 2014; Crundwell et al.,2016; Kozin et al.,2014; Yin et al., 2012). For example, galena flotation was strongly depressed by ferric oxide and alumina particles, but unaffected by kaolinite and gypsum particles. Galena, kaolinite and gypsum used in the research are negatively charged, whereas ferric and alumina were positively charged (Gaudin et al., 1960). Therefore, a deep insight of surface potential is benefit for us to give a better understanding about the flotation mechanism during ascharite flotation process.

Nowadays, most of reported researches about ascharite focus on the separation of ascharite from serpentine and the detrimental effect of serpentine on ascharite flotation performance. However, the surface charge property of ascharite has puzzled researchers for a long time and not reported before. A better understanding of surface charge development of ascharite is crucial for us to know particles interaction behavior and obtain a higher separation efficiency. In addition, the effect of surface charge on particles interaction is also studied, which is benefit for reducing the deterioration of flotation environment.

2.   Materials and methods

Ascharite used in this research was obtained from Dandong, Liaoning province, China. Results of chemical analysis (in Table.1) and XRD (in Fig. 1) confirmed ascharite was of high purity with trace amount of serpentine. The sample was dry ground and screened to -45 μm. Particle size distribution was determined using a Malvern Instruments Mastersizer (Mastersizer2000, England) as shown in Table.2.
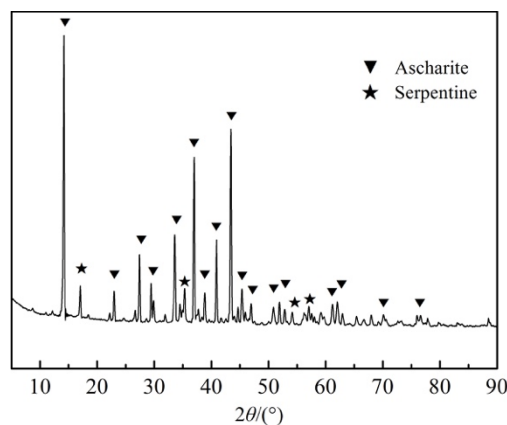
Fig. 1. XRD analysis of ascharite

Table. 1 Chemical analysis results of ascharite ($w/$ %)

Sample	B_2O_3	MgO	SiO_2	Al_2O_3	TFe
Ascharite	39.16	46.21	0.74	0.25	1.87

Table. 2 Particles size distribution of ascharite sample

Sample	$D_{10}/$μm	$D_{50}/$μm	$D_{90}/$μm	Average diameter/μm
Ascharite	1.8	12.1	43.8	27.8

2. Experiments

2.0 g ascharite was added to 20 mL deionized water in a beaker and stirring for 5 min using magnetic stirrer. Then ascharite was separated from suspension liquid by centrifuge, and the concentration of B and Mg in supernatant was detected by ICP analysis. The different dosage of HCl was added into 20 mL ascharite pulp, respectively. After stirring for 5min the slurry was centrifuged, then concentration of B and Mg in centrifugate was analyzed.

2.1 Zeta potential analysis

Ascharite sample was ground to -2 µm, and then 20 mg sample was added into 50 mL deionized water. Potassium nitrate was added into water to maintain ionic strength at 1×10^{-3} mol/L. The suspension was magnetically stirred for 10 min and the pH value was adjusted by using HCl and NaOH. The supernatant was measured using Malvern Zetasizer Nano potential meter 20min later.

2.2 SEM analysis

To give a direct observation to surface of dissolved and undissolved samples, scanning electron microscope was used as an efficient way to analyze the surface morphology. The particles surfaces interaction was studied using SSX-550 scanning electron microscope (Shima-dzu, Japan).

2.3 XPS analysis

For further understanding of the chemistry and physics of mineral/solution interface, X-ray photoelectron spectroscopy was used to prove the change of elements concentration on ascharite surface. The XPS measurements were record with America Thermo VG ESCALAB250 sepectrometer using Al Kα X-rays (1486.6 eV) as sputtering source at a power of 150W (15kV×10 mA). The measurements were performed inside the analysis chamber operating in a high vacuum of 5.0×10^{-7} Pa. In each case the area of analysis was about 700×300 µm². During the data acquisition a system of neutralization of the charge has been used.

3. Results and discussion

3.1 Analysis of dissolution ions from surface

Ascharite, a borate mineral with dimensional layer-like structure along the (0 0 1) plane, is made of a stacking of layers as shown in Fig. 2. Fig. 2(a) and Fig. 2(b) shows that each layer consist of $B_2O_4(OH)$ anionic groups and the isolated Mg atoms and hydroxyls are sandwiched by two layers (Grice, 2008). Each B atom is coordinated with three oxygen atoms to form a BO_3 plane triangle, which connected with adjacent triangular BO_3 group via a bridging oxygen atom to form $B_2O_4(OH)$ with a distorted trigonal structure as shown in Fig. 2(c). Two anionic groups of $B_2O_4(OH)$ are connected by a Mg atom, forming an infinite three-dimensional network along the *a* axis and *b* axis. Mg atoms are surrounded by oxygen atoms or hydroxyl, forming Mg-O octahedron as shown in Fig. 2(d). The octahedron share edges with next one along *c* axis. Furthermore, there are two crystallographic distinct O-H groups in ascharite crystal cells, one type is connected with B atom and another one is bonded with Mg atom. Within the
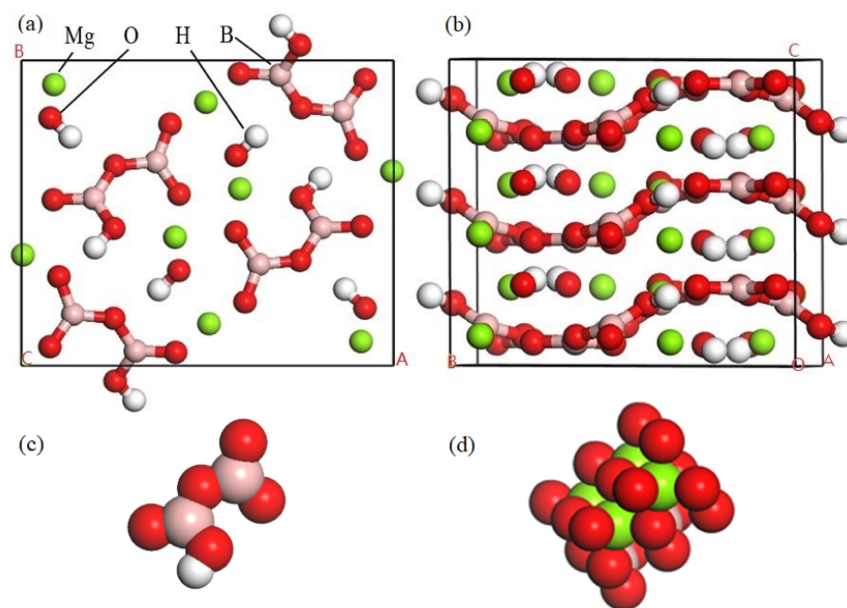
Fig. 2 The crystal structure of ascharite

$B_2O_4(OH)$ anionic groups, the structure is held by covalent bonds and Mg-OH is linked by ionic bond. When these bonds are broken, cleavage in crystal occurs and then neutral faces will be formed on the fracture surfaces. Due to the difference in free energy of hydration of these surface groups, charges on these faces is developed by lattice defects or incongruent dissolution (Frost et al., 2015; Matos et al., 2015; Gao et al., 2016).

For a good understanding of surface charge development of ascharite, solubility studies are carried out to explore the dissolution of cations and anions. As shown in Fig. 3, the concentration of hydroxyl dissolved from ascharite surface is determined by pH values. The pH value of deionized water used in the experiments is 6.4. With time extending, the pH value of slurry increases from 6.4 to 9.5, which corresponding to OH⁻ increased from 2.82×10^{-8} mol/L to 2.82×10^{-5} mol/L. It indicates that the increase of pH value is attributed to the dissolution of hydroxyls.
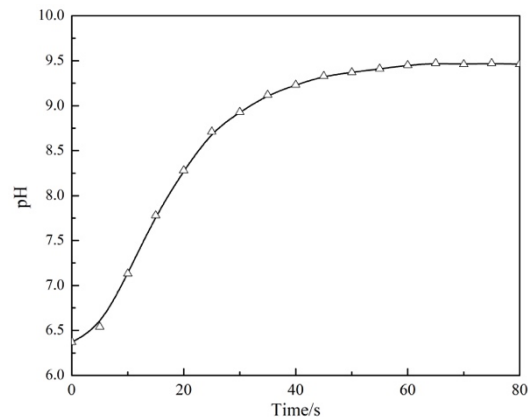
Fig. 3. The pH of ascharite pulp as a function of time

The effect of ascharite mass on ions dissolution is shown in Fig. 4. With addition of ascharite, the element concentration of magnesium and boron increased significantly. In the condition that 2.0 g ascharite dissolves in 20 mL water, the element concentrations of boron and magnesium in centrifugate are 1.4×10^{-4} mol/L and 3.5×10^{-4} mol/L, respectively. Therefore, more cations dissolve into water and more anions are left on surface.
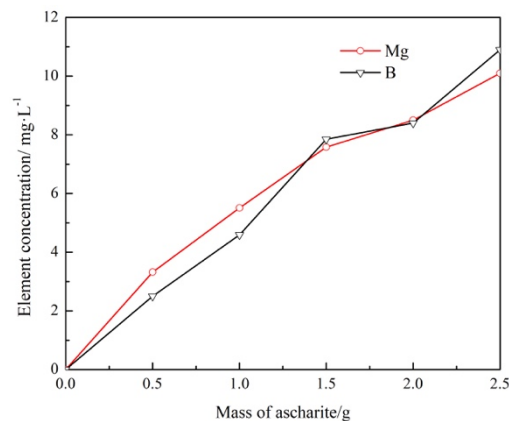
Fig. 4. The effect of mass of ascharite on ions dissolution in water

The dosage effect of HCl on dissolution is shown in Fig. 5. With the increase of HCl dosage, the element concentration of magnesium and boron in solution increase obviously. Furthermore, higher concentration of magnesium is detected in solution, which reveals that more magnesium ions is got rid of the surface of ascharite. It is considered that the transport of magnesium ions from surface to solution is the major trend. The incongruent dissolution of hydroxyl, magnesium ions and borate ions may lead

to the development of surface charge, which is related to the difference in free energy of hydration of these surface groups.
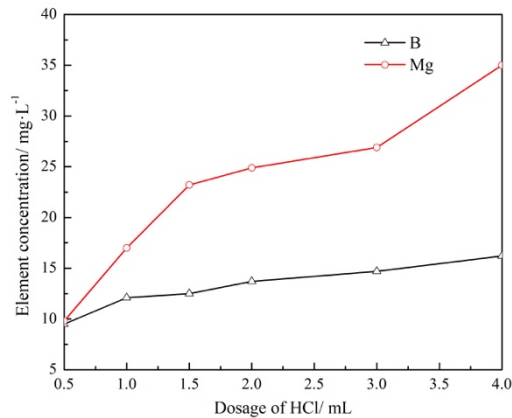
Fig. 5. The effects of HCl dosage on dissolution

3.2 Effects of dissolution and adsorption on Zeta potential

It is a widespread acceptance that Zeta potential has a significant effect on surface property (Dultz et al., 2018; Philipp et al., 2014). The Zeta potential analysis result of ascharite is shown in Fig. 6. With the increase of pH values, Zeta potential of original ascharite decreases gradually and it has an isoelectric point (IEP) of pH 7.6. The Zeta potential of leached ascharite (the ascharite samples treated by HCl solution) is more negative and the IEP is about pH 3.9. It indicates that the surface potential of leached ascharite is dominated by negative charges, so it is considered that more cations dissolve in this process.

Because much more magnesium ions are removed from surface, so the surface of leached ascharite is more negative charged. Then, the influence about magnesium ions on surface potential is discussed. After treated by 1.4×10^{-3} mol/L Mg^{2+}, Zeta potential of leached ascharite increases prominently and IEP change to 6.7 and 10.8(shown in Fig. 6).
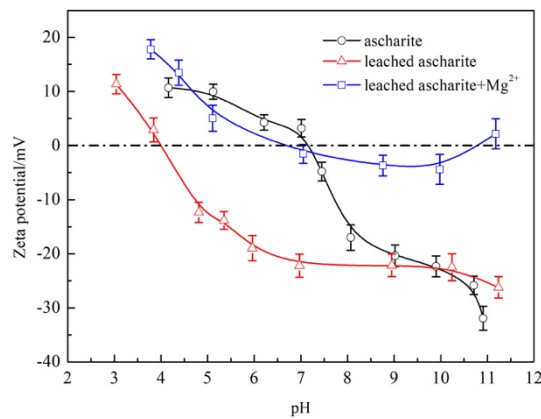
Fig. 6. Zeta potential analysis of ascharite

As discussed above, Mg^{2+} has an important effect on the development of surface potential, but there are more details about how it influences surface potential need to be further discussed. The species distribution of Mg^{2+} (1.4×10^{-3} mol/L) is listed in Fig. 7. Mg^{2+} can react with the hydroxyl kept on the surface, resulting in the formation of $Mg(OH)^+$ and $Mg(OH)_{2(s)}$. As a result, the positive charges increase remarkably and even precipitation is formed at pH of 10.8. Because of the adsorption of large amount of Mg^{2+}, the surface potentials even change from negative to positive (shown in Fig. 6). The result of species distribution is consistent with that of Zeta potential analysis. Therefore, the influence of incongruent dissolution caused by excessive dissolution of magnesium cations takes great effect on development of surface charge.
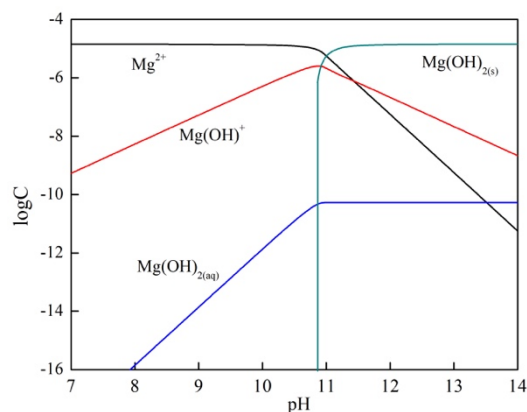
Fig. 7. The species distribution of Mg^{2+} (1.4×10^{-3} mol/L)

3.3 Surface component of ascharite after dissolution

By invoking the assumption that dissolution of various groups occurs on surface, the component of ascharite surface is detected by XPS. The XPS analysis results in different condition are shown in Table.3. The carbon concentrations are not necessarily representative of ascharite samples due to the air exposure of samples before analysis (Shchukarev et al., 2005; Schulze et al., 2004; Liu et al., 2016). It indicates that elements content on the surface of ascharite change obviously after treated with water or acid solution. When compared with the composition of the original ascharite, the contents of B and Mg on surfaces treated by water are reduced from 16.86% to 16.7% and from 16.1% to 15.02%, respectively. Besides, the transport of B and Mg from ascharite surface to HCl solution is more obvious than that in water, which is consistent with the experimental data. Furthermore, more magnesium ions are removed from the surface, resulting in the charging of ascharite surface. The results demonstrate that the removal of materials from ascharite surface caused by dissolution leads to the development of surface potential.

Table. 3 Mole fraction of elements on surface of ascharite samples by XPS/ %

Samples	C	O	B	Mg
Ascharite	15.0	52.22	16.86	16.1
Ascharite+H_2O	16.05	52.23	16.7	15.02
Ascharite+HCl	25.61	48.83	15.06	10.5

3.4 Dissolution process of surface groups

The SEM images in Fig. 8 show that the surface topography and microstructure of ascharite have a significant change after dissolution. The ascharite particles exhibit a smooth surface in Fig. 8(a) and it becomes bumpy after treated by water and acid with a stirring time of 10 min as illustrated in Fig. 8(b) and Fig. 8(c). The effect of HCl on surface microstructure is more remarkable than that of water, which means that the dissolution rate may be accelerated by HCl. The EDS spectrum in Fig. 8 shows that a phase composed of Mg with minor amounts of Fe. The presence of Fe suggests the possibility of a partial substitution of Mg^{2+} by cations with similar ionic radius like Fe^{3+}. Furthermore, due to the isomorphous substitution of Fe^{3+} for Mg^{2+} in the Mg-O octahedron sheet, it has been commonly assumed that the basal plane of layered octahedron sheets carry a permanent positive charge. However, the effect of isomorphous substitution on surface charging behavior is not obvious.

As discussed above, ascharite can dissolve in aqueous solution and surface charge property is changed. Then the groups on surface is considered to change dramatically after dissolution. For further understanding of the transport of groups from surface to solution, the dissolution process is illustrated schematically in Fig. 9.
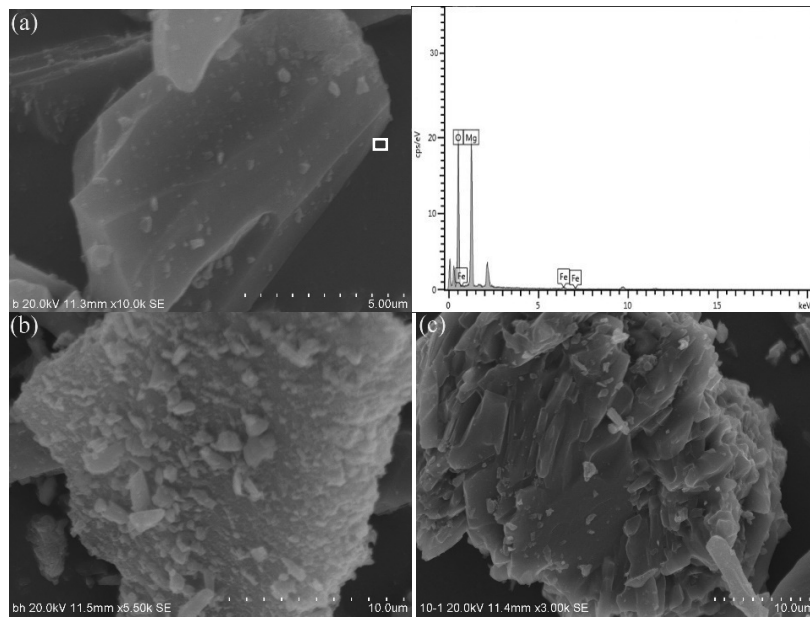
Fig. 8. SEM images and EDS spectrum of ascharite surface (a: original sample; b: sample treated by water; c: sample treated by HCl)
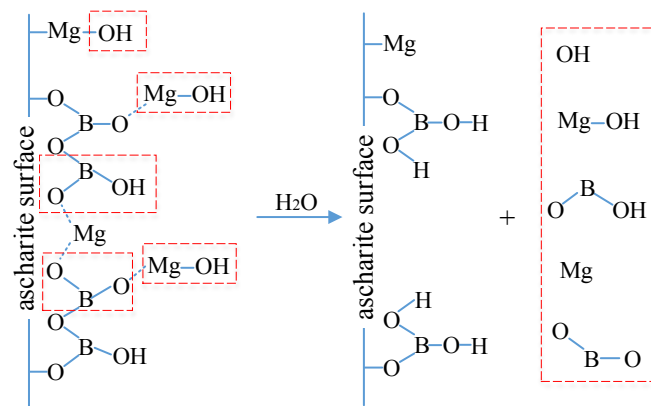
Fig. 9. Dissolution process of ascharite in solution

Two different type of OH groups are observed in the ascharite crystal structure, one is bonded with Mg atom and another one is associated with B atom. The increase of pH is most likely to be caused by dissolution of hydroxyl. The atoms are covalently linked in B-O structure and atoms are interconnected by ionic bonds in Mg-OH groups. When these bonds are broken, amount of magnesium ions, hydroxyl and borate ions transport from surface to water, leading to the increases of pH values and concentrates of B and Mg (shown in Fig. 3 and Fig. 4). The boric acid is formed on ascharite surface after the ionization of OH- from B(OH)4- groups.

The main chemical reactions represent elementary steps in dissolution mechanism, following expressions are considered for the removal of ions from ascharite surface and the formation of boron acid.

$$Mg_2[B_2O_4(OH)]OH + 4H_2O = 2B(OH)_4^- + 2Mg^{2+} + 2OH^- \qquad (1)$$

$$B(OH)_4^- = H_3BO_3 + OH^- \qquad (2)$$
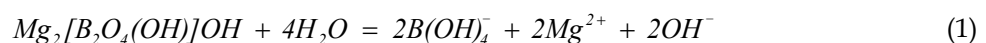
3.5 Effect of surface charge property on particles aggregation

The surface charging behaviors are determined by DLVO theory. The formation of slime coating is controlled by interaction energy between slime and mineral particles and involves the aggregation

process (Yu et al., 2017). Interactions between mineral particles are generally controlled by van der Waals forces and electrostatic interaction, which can be quantitatively predicted by DLVO theory (Sinha et al., 2013; Yu et al., 2018). Previous research shows that floatation performance of ascharite can be depressed by fine serpentine particles, this is may be caused by the particles interaction between ascharite and serpentine (Li et al., 2017). References showed that van der Waals forces are generally attractive forces widely existing between mineral particles, and electrostatic force was the main reason leading to serpentine slime adhesion to mineral surfaces (Bremmell et al., 2005). Based on the DLVO theory and previous references, surface charge of mineral particles has an important effect on particles interactions.

The effect of surface charge property on particles interaction is analyzed by DLVO theory, which can make a prediction of particles interaction behavior. A constant charge boundary condition is applied in DLVO theory analysis in this research. The total interaction energy is shown as following equation (Wang et al., 2015; Hartmann et al., 2018):

$$V_T = V_W + V_E \tag{3}$$

where V_T, V_W, V_E are the total energy, van der Waals energy and electrostatic energy, respectively.

The van der Waals energy can be described as

$$V_W = -\frac{AR_1R_2}{6H(R_1 + R_2)} \tag{4}$$

where R is the radius of mineral particle; H represents separation distance between particles; A is Hamaker constant of two different minerals in aqueous solution and it can be described as follow:

$$A = (\sqrt{A_{11}} - \sqrt{A_{33}})(\sqrt{A_{22}} - \sqrt{A_{33}}) \tag{5}$$

where A_{11}, A_{22} represent Hamaker constant of minerals in vacuum. The Hamaker constants of ascharite is 19.3×10^{-20} J and 10.3×10^{-20} J in vacuum condition, respectively. (Li et al., 2017). A_{33} represents the Hamaker constant of water in vacuum, $A_{33} = 4.15 \times 10^{-20}$ J(Lu et al., 2015). Therefore, the Hamaker constant for ascharite and serpentine in aqueous solution, $A_1 = 2.76 \times 10^{-20}$ J; The electrostatic energy can be calculated as

$$V_E = \frac{\pi \varepsilon_a R_1 R_2}{R_1 + R_2}\left(\varphi_1^2 + \varphi_2^2\right)\left(\frac{2\varphi_1\varphi_2}{\varphi_1^2 + \varphi_2^2} \times \ln\frac{1 + e^{-\kappa H}}{1 - e^{-\kappa H}} + \ln\left(1 - e^{-\kappa H}\right)\right) \tag{6}$$

where κ is the reciprocal of the thickness of electric double-layer, $\kappa = 0.180$ nm^{-1}(Lu et al., 2011); ε_a is the relative dielectric constant of the continuous phase, $\varepsilon_a = 6.95 \times 10^{-10}$ C^2/(J·m) (Wang et al., 2016); φ_1 and φ_2 are surface potential, mv. The radii of ascharite and serpentine used here are about 20 μm. The Zeta potential of serpentine and ascharite based on the experimental data is listed in Table.4.

Table. 4 Zeta potential of ascharite and serpentine at pH of 5 and 11

pH	Serpentine/mV	Ascharite/mV	Leached ascharite/mV
5	18.2	9.7	-14.8
11	-16.3	-33.5	-25.7

The curves of total interaction energy are shown in Fig. 10. It displays the variation tendency of interaction energy between mineral particles in different condition.

The total energy between serpentine and ascharite particles is negative at pH of 5, which indicates that force between serpentine and ascharite particles shows attractive. Furthermore, total interaction energy between serpentine and leached ascharite is more negative at pH of 5, indicating that particles aggregation is easy to occur in this condition. The similar results are found at pH of 11. The positive interaction energy between serpentine and ascharite at pH 11 indicates that serpentine particles will be dispersed with ascharite. However, the interaction energy decreases after ascharite dissolving in water,

so the well dispersed state between mineral particles is weakened at pH of 11. Particles aggregation is also not benefit to the floatation process. Therefore, it can be found that dissolution of ascharite, resulting in a dramatic change of surface charge, has a detrimental effect on the dispersion of mineral particles.
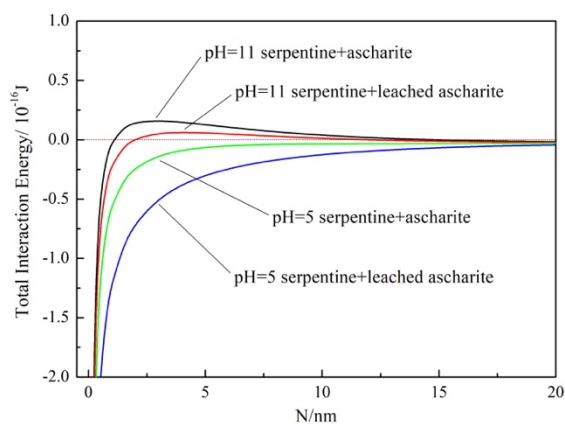
Fig. 10 Total interaction energy between serpentine and ascharite particles

4.   Conclusions

The incongruent dissolution of ascharite is prone to occur when it is put in aqueous solution. As a result of the incongruent dissolution of cations with respect to anions, surface becomes more negatively charged. The incongruent dissolution is attributed to the disparity in the bonding energy of B–O and Mg–OH and the difference in free energy of hydration of surface groups. Besides, isomorphous substitution of Fe^{3+} for Mg^{2+} in the Mg-O octahedron sheet is regarded as another factor that influences surface-charging behavior, but the isomorphous substitution is not the major factor. Therefore, in this research the surface charging behavior of ascharite is caused by incongruent dissolution and isomorphous substitution.

The effect of incongruent dissolution of ascharite on particles interaction is analyzed by DLVO theory. The result shows that dissolution of ascharite can lead to a trend of particles aggregation, which will result in a deterioration of floatation environment.

Acknowledgements

References

BREMMELL, K.E., FORNASIERO D., RALSTON J., 2005. *Pentlandite-lizardite interactions and implications for their separation by flotation*. Colloids and Surfaces A-physicochemical and Engineering Aspects. 252(2/3), 207-212.

CRUNDWELL, F.K., 2016. *The mechanism of dissolution of minerals in acidic and alkaline solutions: Part V surface charge and zeta potential*. Hydrometallurgy. 161,174-184.

DULTZ, S., STEINKE, H., MIKUTTA, R., WOCHE, S.K., GUGGENBERGER, G., 2018. *Impact of organic matter types on surface charge and aggregation of goethite*. Colloids and Surfaces A. 554, 156-168.

FENG, B., FENG, Q., LU, Y., 2012. *A novel method to limit the detrimental effect of serpentine on the flotation of pentlandite*. International Journal of Mineral Processing. 114, 11-13.

FROST, R.L., SCHOLZ, R., LOPEZ, A., BELOTTI, F.M., 2015. *The molecular structure of the borate mineral szaibelyite MgBO2(OH)–A vibrational spectroscopic study*. Journal of Molecular structure. 1089, 20-24.

FURRER, G., STUMM, W., 1988. *The coordination chemistry of weathering: I. Dissolution kinetics of δ-Al2O3 and BeO*. Geochimica et Cosmochimica Acta. 50, 1847–1860.

FU, X., ZHAO, J., CHEN, S., LIU, Z., GUO, T., CHU, M., 2015. *Comprehensive Utilization of Ludwigite Ore Based on Metallizing Reduction and Magnetic Separation*. Journal of iron and steel research international. 22(8), 672-680.

GALLIOS, G.P., DELIYANNI, E.A., PELEKA, E.N., MATIS, K.A., 2007. *Flotation of chromite and serpentine.* Separation and Purification Technology. 55, 232-237.

GAO, R., LIU, Q., WANG, J., ZhANG, X., YANG, W., LIU, J., LIU, L., 2014. *Fabrication of fibrous szaibelyite with hierarchical structure superhydrophobic coating on AZ31 magnesium alloy for corrosion protection.* Chemical Engineering Journal, 241, 352-359.

GAO, Z., LI, C., HU, Y., 2017. *Anisotopic surface properties of calcite: A consideration of surface broken bonds.* Colloids and Surfaces A: Physicochemical and Engineering Aspects. 520, 53-61.

GAO, Z., HU, Y., SUN, W., DRELICH J.W., 2016. *Surface-Charge Anisotropy of Scheelite Crystals.* Langmuir. 32(25), 6282-6288.

GAUDIN, A.M., FUERSTENAU, D.W., MIAW, H.L., 1960. *Slime coatings in galena flotation.* Trans. Can. Inst. Min. Metal. 63, 668–671.

GRICE, J.D., 2008. *Szaibelyite: crystal structure analysis and hydrogen bonding.* The Canadian Mineralogist. 46, 671-677.

GUPTA, V., HAMPTON, M.A., STOKES, J.R., NGUYEN, A.V., MILLER, J.D., 2011. *Particle interactions in kaolinite suspensions and corresponding aggregate structures.* Journal of Colloid and Interface Science. 359, 85-103.

HARTMANN, R., KINNUNEN, P., ILLIKAINEN, M., 2018. *Cellulose-mineral interactions based on the DLVO theory and their correlation with flotability.* Minerals Engineering. 122, 44-52.

KOZIN, P.A., BOILY, J.F., 2014. *Mineral surface charge development in mixed electrolyte solutions.* Journal of Colloid and Interface Science. 418, 246-253.

KUSUMA, A.M, LIU, Q., ZENG, H., 2014. *Understanding interaction mechanisms between pentlandite and gangue minerals by zeta potential and surface force measurements.* Minerals Engineering. 69,16-23.

LIANG, B., LI, G., RAO, M., PENG, Z., ZHANG, Y., JIANG, T., 2017.*Water leaching of boron from soda-ash-activated ludwigite ore.* Hydrometallurgy. 167, 101-106.

LIU, C., ZHANG, W., SONG, S., LI, H., 2019. *Effect of lizardite on pentlandite flotation at different pH: Implications for the role of particle-particle interaction.* Minerals Engineering. 132, 8-13.

LIU, W., LIU, W., WANG, X., WEI, D., WANG, B., 2016. *Utilization of novel surfactant N-dodecyl-isopropanolamine as collector for efficient separation of quartz from hematite.* Separation and Purification Technology. 162,188-194.

LI, Y., HAN, Y., ZHU, Y., 2007. *Study on the Characteristic of Camsellite Flotation.* Journal of Northeastern University (natural Science). 28(7), 1041-1045.

LI, Z., HAN, Y., GAO, P., YING, P., 2016. *Research on Processing Mineralogical Characterization of the Paigeite Ore.* Journal of Northeastern University (Natural Science). 37(2), 258-262.

LI, Z., HAN, Y., LI, Y., GAO, P., 2017. *Interaction between mineral particles during ascharite flotation process and direct force measurement using AFM.* Physicochemical Problems of Mineral Processing. 53(2),1161-1174.

LI, Z., HAN, Y., LI, Y., GAO, P., 2017. *Effect of serpentine and sodium hexametaphosphate on ascharite flotation.* Transactions of Nonferrous Metals Society of China. 27,1841-1848.

LU, J. YUAN, Z., LIU, J., LI, L., ZHU, S., 2015. *Effects of magnetite on magnetic coating behavior in pentlandite and serpentine system.* Minerals Engineering. 72,115-120.

LU, Y., ZHANG, M., FENG, Q., LONG, T., OU, L., ZHANG, G., 2011. *Effect of sodium hexametaphosphate on separation of serpentine form pyrite.* Transactions of Nonferrous Metals Society of China. 21,208-213.

MATOS, M., TERRA, J., ELLIS, D.E., PIMENTEL, A.S., 2015. *First principles calculation of magnetic order in a low-temperature phase of the iron ludwigite.* Journal of Magnetism and Magnetic Materials. 374,148-152.

OELKERS, E.H., SCHOTT, J., DEVIDAL, J.L., 1994. *The effect of aluminum, pH, and chemical affinity on the rates of aluminosilicate dissolution rates.* Geochimica et Cosmochimica Acta. 58, 2011-2024

PHILIPP, A.K., BOILY, J-F., 2014. *Mineral surface charge development in mixed electrolyte solutions.* Journal of Colloid and Interface Science. 418, 246-253.

SCHULZE, R.K., HILL, M.A., FIELD, R.D., RAPIN, P.A., HANRAHAN, R.J., BYLER, D.D., 2004. *Characterization of carbonated serpentine using XPS and TEM,* Energy Conversion and Management. 45(20), 3169-3179.

SHAW, D.J., 1969. *Electrophoresis.* New York: Academic Press, pp.151-156.

SHCHUKAREV, A., SJOBERG, S., 2005. *XPS with fast-frozen samples: A renewed approach to study the real mineral/solution interface.* Surface Science. 584(1), 106-112.

SINHA, P., SZILAGYI, I., RUIZ-CABELLO, F.J.M., MARONI, P., BORKOVEC, M., 2013. *Attractive forces between charged colloidal particles induced by multivalent ions revealed by confronting aggregation and direct force measurements.* Journal of Physical Chemistry Letters. 4,648-652.

VERMILYEA, D.A., 1966. *The dissolution of ionic compounds in aqueous media.* Journal of the Electrochemical Society. 113, 1067-1070.

WANG C., WANG H., GU G., FU J., LIN Q., LIU Y.,2015, *Interfacial interactions between plastic particles in plastics flotation*, Waste Management, 46,56-61.

WEI, R., PENG, Y., SEAMAN, D., 2013. *The interaction of lignosulfonate dispersants and grinding media in copper–gold flotation from a high clay ore.* Mineral Engineering. 50-51, 93-98.

YIN, X., GUPTA, V., DU, H., WANG, X., Miller, J.D., 2012. *Surface charge and wetting characteristics of layered silicate minerals.* Advances in Colloid and Interface Science. 179, 43-50.

YU, Y., MA, L., CAO, M., LIU, Q., 2017. *Slime coatings in froth floatation: A review.* Minerals Engineering. 114, 26-36.

YU, Y., MA, L., XU, H., SUN, X., ZHANG, Z., YE, G., 2018. *DLVO theoretical analyses between montmorillonite and fine coal under different pH and divalent cations.* Power Technology. 330,147-151.

ZHAO, R., HAN, Y., YANG, G., LI, Y., 2015. *Mechanism of Adsorption and Aggregation of Fine Siderite, Quartz and Hematite.* Journal of Northeastern University (Natural Science). 36(4), 596-600.

ZHOU, X., FENG, B., 2015. *The effect of polyether on the separation of pentlandite and serpentine.* Journal of Materials Research and Technology. 4(4), 429-433.

ZHU, Y., LUO, B., SUN, C., LI, Y., HAN, Y., 2015. *Influence of bromine modification on collecting property of lauric acid.* Mineral Engineering. 79, 24-30.